

Surface reconstruction modulated superconductivity on quasi-2D iron pnictide superconductor $KCa_2Fe_4As_4F_2$

Wenjing Zeng(曾文静), Zongyuan Zhang(张宗源), Xiaoyan Dong(董晓燕), Yubing Tu(涂玉兵), Yanwei Wu(吴彦玮), Teng Wang(王腾), Fan Zhang(张凡), Shuai Shao(邵帅), Jie Hou(侯杰), Xingyuan Hou(侯兴元), Ning Hao(郝宁), Gang Mu(牟刚), and Lei Shan(单磊)

Citation: Chin. Phys. B, 2025, 34 (**8**): 087402. DOI: 10.1088/1674-1056/add5cb
http://cpb.iphy.ac.cn; http://iopscience.iop.org/cpb

What follows is a list of articles you may be interested in

Dimensional crossover from quasi-2D to 3D superconductivity in (Li,Fe)OHFeSe$_{1-x}$S$_x$ driven by chemical pressure

Yuxin Ma(马宇欣), Munan Hao(郝木难), Qi Li(李琦), Ke Ma(马克), Haodong Li(李浩东), Duo Zhang(张铎), Ruijin Sun(孙瑞锦), Shifeng Jin(金士锋), and Changchun Zhao(赵长春)
Chin. Phys. B, 2025, 34 (**6**): 067402. DOI: 10.1088/1674-1056/adc404

Coevolution of superconductivity and Hall coefficient with anisotropic lattice shrinkage in compressed $KCa_2Fe_4As_4F_2$

Jinyu Han(韩金宇), Wenshan Hong(洪文山), Shu Cai(蔡树), Jinyu Zhao(赵金瑜), Jing Guo(郭静), Yazhou Zhou(周亚洲), Pengyu Wang(王鹏玉), Lixin Cao(曹立新), Huiqian Luo(罗会仟), Shiliang Li(李世亮), Qi Wu(吴奇), and Liling Sun(孙力玲)
Chin. Phys. B, 2024, 33 (**7**): 077402. DOI: 10.1088/1674-1056/ad4d65

Co-doped $BaFe_2As_2$ Josephson junction fabricated with a focused helium ion beam

Ziwen Chen(陈紫雯), Yan Zhang(张焱), Ping Ma(马平), Zhongtang Xu(徐中堂), Yulong Li(李宇龙), Yue Wang(王越), Jianming Lu(路建明), Yanwei Ma(马衍伟), and Zizhao Gan(甘子钊)
Chin. Phys. B, 2024, 33 (**4**): 047405. DOI: 10.1088/1674-1056/ad21f7

Distinct behavior of electronic structure under uniaxial strain in $BaFe_2As_2$

Jiajun Li(李佳俊), Giao Ngoc Phan, Xingyu Wang(王兴玉), Fazhi Yang(杨发枝), Quanxin Hu(胡全欣), Ke Jia(贾可), Jin Zhao(赵金), Wenyao Liu(刘文尧), Renjie Zhang(张任杰), Youguo Shi(石友国), Shiliang Li(李世亮), Tian Qian(钱天), and Hong Ding(丁洪)
Chin. Phys. B, 2024, 33 (**1**): 017401. DOI: 10.1088/1674-1056/acd8af

Focused-ion-beam assisted technique for achieving high pressure by uniaxial-pressure devices

Di Liu(刘迪), Xingyu Wang(王兴玉), Zezhong Li(李泽众), Xiaoyan Ma(马肖燕), and Shiliang Li(李世亮)
Chin. Phys. B, 2023, 32 (**4**): 047401. DOI: 10.1088/1674-1056/acac1a

---

Surface reconstruction modulated superconductivity on quasi-2D iron pnictide superconductor $KCa_2Fe_4As_4F_2$

Wenjing Zeng(曾文静)[1], Zongyuan Zhang(张宗源)[1,2,†], Xiaoyan Dong(董晓燕)[1], Yubing Tu(涂玉兵)[1,2], Yanwei Wu(吴彦玮)[1], Teng Wang(王腾)[3], Fan Zhang(张凡)[5], Shuai Shao(邵帅)[1], Jie Hou(侯杰)[1,2], Xingyuan Hou(侯兴元)[1,2], Ning Hao(郝宁)[4], Gang Mu(牟刚)[3,‡], and Lei Shan(单磊)[1,2,§]

[1] *Information Materials and Intelligent Sensing Laboratory of Anhui Province, Leibniz International Joint Research Center of Materials Sciences of Anhui Province, Anhui University, Hefei* 230601, *China*

[2] *Center of Free Electron Laser and High Magnetic Field, Institutes of Physical Science and Information Technology, Hefei* 230601, *China*

[3] *State Key Laboratory of Materials for Integrated Circuits, Shanghai Institute of Microsystem and Information Technology, Chinese Academy of Sciences, Shanghai* 200050, *China*

[4] *Anhui Provincial Key Laboratory of Low-Energy Quantum Materials and Devices, High Magnetic Field Laboratory, HFIPS, Chinese Academy of Sciences, Hefei* 230031, *China*

[5] *Beijing National Laboratory for Condensed Matter Physics, Institute of Physics, Chinese Academy of Sciences, Beijing* 100190, *China*

(Received 20 March 2025; revised manuscript received 23 April 2025; accepted manuscript online 8 May 2025)

Iron-based superconductors (FeSCs) feature a complex phase diagram, and their diverse cleavage terminations offer a versatile platform for modulating surface electronic states and investigating the underlying superconducting mechanisms. In this study, we explore the surface modulation of $KCa_2Fe_4As_4F_2$ using scanning tunneling microscopy/spectroscopy. Cryogenically cleaved surfaces reveal multiple configurations, including $\sqrt{2}\times\sqrt{2}$ reconstruction, 1×2 and 1×3 stripes, as well as nanoscale vacancies. Reducing potassium coverage induces hole doping, which shifts the density of states peak toward the Fermi level and suppresses the superconducting gap from 4.8 meV to 3.2 meV. This behavior is reminiscent of the Van Hove singularity observed in hole-doped 122-type FeSCs. The band structure does not undergo a simple rigid shift, and the evolution of superconductivity can be attributed to the interplay between surface carriers and electronic correlations. Additionally, a V-shaped gap is observed at a unique location preserving the FeAs bilayer structure, where interlayer coupling effects are likely involved. The diversity of surface structures and electronic states in K12442 enhances our understanding of FeSCs and facilitates the modulation and application of FeAs superconducting layers.

Keywords: iron-based superconductor, surface reconstruction, carrier doping, van Hove singularity, electronic correlation

PACS: 74.55.+v, 73.25.+i, 74.25.–q, 07.79.Cz

DOI: 10.1088/1674-1056/add5cb **CSTR:** 32038.14.CPB.add5cb

Iron-based superconductors (FeSCs), characterized by moderate electron correlation and multi-band features, not only exhibit a complex phase diagram but also provide a unique platform for exploring unconventional superconductivity.[1–4] Their intricate band structure makes them highly responsive to various external modulations. For example, in $BaFe_2As_2$ (122 system), electron doping via Co substitution for Fe, hole doping through K, or even isovalent substitution of As by P can suppress the orthorhombic antiferromagnetic ground state, resulting in a dome-shaped superconducting region in the phase diagram.[5,6] Additionally, pressure-induced superconductivity in 122 system under hydrostatic condition and its extreme sensitivity to uniaxial stress have been widely reported.[7,8] Moreover, extensive charge carrier modulations offer a framework for interpreting the phase diagram of FeSCs by treating electron correlation or bandwidth as universal parameters.[9,10] As layered structures, FeSCs can be precisely fabricated layer-by-layer using molecular beam epitaxy or mechanically exfoliated to reduce dimensionality,[11–15] facilitating the study of the basic superconducting units such as FeSe or FeAs layers.

FeSCs with natural cleavage planes, such as FeSe and LiFeAs, typically exhibit nonpolar and fully intact atomic lattices at their termination surfaces.[16,17] In contrast, systems without natural cleavage layers, including $BaFe_2As_2$, $CaKFe_4As_4$, and $KCa_2Fe_4As_4F_2$,[18–22] display multiple metastable termination configurations, which depend on specific cleavage conditions like temperature and annealing procedures.[23–25] For example, the cleavage surfaces of the 122 system can include dimerized As surfaces, $(\sqrt{2}\times\sqrt{2})R45°$ or 1×2 reconstructions of alkaline-earth atoms, and occasionally exposed Fe termination layer.[24] Using STM/STS techniques, researchers have discovered

†Corresponding author. E-mail: zongyuanzhang@ahu.edu.cn
‡Corresponding author. E-mail: mugang@mail.sim.ac.cn
§Corresponding author. E-mail: lshan@ahu.edu.cn

© 2025 Chinese Physical Society and IOP Publishing Ltd. All rights, including for text and data mining, AI training, and similar technologies, are reserved.

termination-dependent superconductivity and orbital-selective tunneling processes on these different surfaces.[23–25] Subsequent studies have further demonstrated that surface disorder can induce superconductivity in $BaFe_2As_2$.[26] In addition to the effects of carrier concentration and disorder scattering, the role of electron correlation on symmetry-breaking cleavage surfaces has also been proposed.[27] These findings highlight the tunable nature of superconductivity on FeSCs surfaces. However, due to interlayer coupling or the distinct properties of individual surfaces, a clear and unified understanding of the modulation mechanisms in the FeAs layer remains elusive. In the $KCa_2Fe_4As_4F_2$ (K12442) system, the significant anisotropic resistance ratio $\rho_c/\rho_{ab} \sim 10^3$ suggests weak interlayer coupling between the separated bilayer FeAs blocks.[28–33] Additionally, the out-of-plane coherence length $\xi_c(0)$ is estimated to be smaller than the interbilayer distance, further confirming the two-dimensional (2D) nature of the 12442 system.[34] Recently, combined STM/STS and bulk transport measurements have shown that the FeAs monolayer on the cleavage surface of K12442 is effectively isolated from the bulk material by the underlying CaF insulating layer.[20] This unique configuration provides an ideal opportunity to study and manipulate the basic superconducting unit — the FeAs layer.

In this work, we investigate the surface modulation of K12442. Low-temperature cleavage generates surfaces with varying K coverage, enabling the tunning of surface carrier. The reduction in K coverage induces hole doping effect, which shifts the DOS peak toward the Fermi level (E_F), similar to the Van Hove singularity (VHS) observed in hole-doped 122-type FeSCs.[35] Meanwhile, the superconducting gap is also suppressed from 4.8 meV to 3.2 meV. In the FeAs bilayer region, carrier modulation is also observed, accompanied by a V-shaped gap structure likely attributed to interlayer coupling effects. These findings demonstrate that the FeAs layers in quasi-2D K12442 are highly sensitive to carrier doping and electron correlation effects.

K12442 single crystals are synthesized by the self-flux method.[36] The samples are characterized by electrical resistivity and magnetic susceptibility measurements, showing a T_c onset of about 33.5 K with a transition width of ~ 1 K, consistent with samples used in our STM/STS study.[20] STM/STS experiments are performed in a low-temperature scanning tunneling microscope (USM-1300, Unisoku). The samples are cleaved in an ultrahigh vacuum at either room temperature or 77 K and then transferred to the STM head maintained at around 4.2 K. Electrochemically etched tungsten tips are used after electron-beam heating and calibrating on the Au (111) surface. Tunneling spectra are obtained using a standard lock-in technique.

Figure 1(a) illustrates the structural model of K12442, where the bilayer FeAs blocks and the insulating CaF layers are alternately stacked to form a sandwich structure.[30] Cleavage typically occurs at the K layer, which splits the FeAs bilayers.[20,21,31,37] Moreover, the FeAs layers on the termination are separated from the bulk by the underlying CaF buffer, creating a relatively isolated FeAs layer (see the structure diagrams in Fig. 1(a) and Fig. 4(a)).[20] This offers an opportunity to study and manipulate the basic superconducting FeAs unit. Figure 1(b) displays the typical STM topography of K12442 cleaved at room temperature. The atomically resolved inset reveals a uniform $\sqrt{2} \times \sqrt{2}$ reconstruction relative to the bulk K layer, except for sporadic atomic vacancies, consistent with observations on other alkali metal-terminated surfaces like Cs.[38] In 122-type FeSCs, cleavage surfaces often display multiple metastable configurations that modulate surface superconductivity, motivating a detailed study of quasi-2D K12442. Figure 1(c) presents a representative topography of the low-temperature cleavage at 77 K, showcasing diverse K layer configurations. Dashed lines in Fig. 1(c) highlight two main regions: the $\sqrt{2} \times \sqrt{2}$ structure, similar to that in Fig. 1(b), and a newly emerged 2×1 stripe order, with a magnified view in the inset. Other minor configurations, such as 3×1 stripes and nanoscale K vacancies, are detailed in Figs. 2(f) and 2(g), respectively.

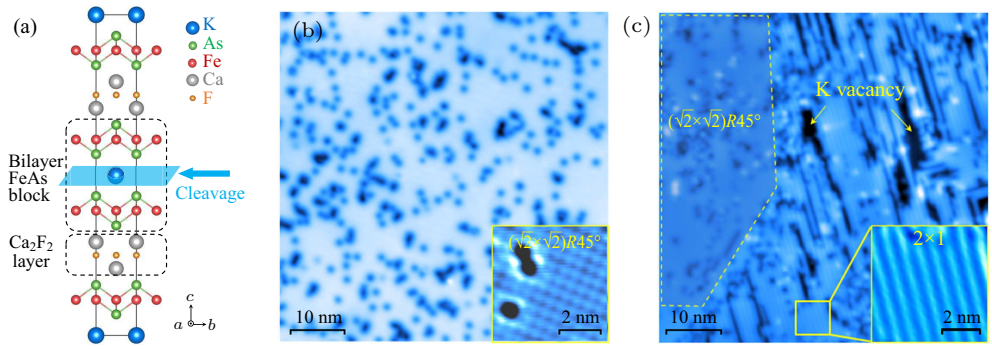


Fig. 1. (a) Lattice structure of K12442. (b) A typical STM image on K12442 cleaved at room temperature ($V_{set} = -120$ mV, $I_t = 10$ pA, size 60 nm×60 nm). The inset shows a uniform $\sqrt{2} \times \sqrt{2}$ lattice of half-K surface, accompanied by a sparse distribution of atomic vacancies. (c) A representative STM image cleaved at low temperature of 77 K ($V_{set} = -100$ mV, $I_t = 20$ pA, size 60 nm×60 nm). The cleavage plane exhibits $\sqrt{2} \times \sqrt{2}$ surface, stripe structures, and nanoscale K vacancies simultaneously.

Figures 2(a)–2(c) illustrate the structural models of $\sqrt{2}\times\sqrt{2}$, 2×1, and 3×1 reconstructions, respectively, with their corresponding STM images shown in Figs. 2(d)–2(f). The topography of nanoscale K vacancies is shown in Fig. 2(g). These configurations can be clearly identified from the cross-sectional height profiles, the spacing between the stripes, and the symmetric relationship where the stripes form a 45° angle with the $\sqrt{2}\times\sqrt{2}$ structure. After identifying these structures, we statistically collected $\mathrm{d}I/\mathrm{d}V$ spectra at representative locations (Figs. 2(h)–2(k)). The gap values, determined by superconducting coherence peaks, are summarized in Fig. 2(l). The gap sizes on the $\sqrt{2}\times\sqrt{2}$ and 2×1 structures are similar ($\sim$ 4.8 meV), with only variation in the height of coherence peaks (Figs. 2(h) and 2(i)). Given their equivalent K-coverage and carrier concentration on $\sqrt{2}\times\sqrt{2}$ and 2×1 surfaces (Figs. 2(a) and 2(b)), the decay of coherent peaks may be influenced by the scattering potential of specific reconstructions, further highlighting the sensitivity and tunability of the superconductivity on K12442 surface. In contrast, the gap sizes on the 3×1 stripes and nanoscale K vacancies show a notable reduction, falling below 3.2 meV. To gain deeper insights into how variations in electronic states impact superconductivity, we analyze the spectra across a wider energy range, as illustrated in Fig. 3.

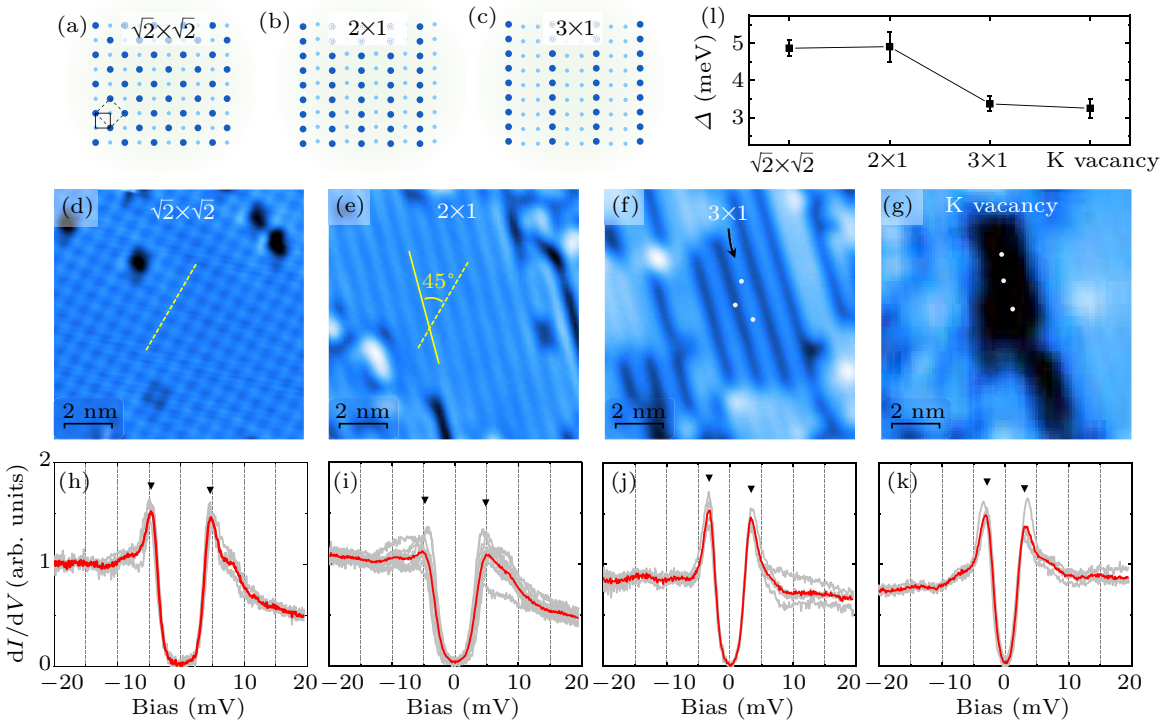


Fig. 2. (a)–(c) Schematic diagrams of the $\sqrt{2}\times\sqrt{2}$, 2×1, and 3×1 structures, respectively. The small solid-line square represents the 1×1 K lattice identical to that in the bulk, while the large dashed-line square denotes the $\sqrt{2}\times\sqrt{2}$ structure on the half-K terminated surface. (d)–(g) The typical STM images of $\sqrt{2}\times\sqrt{2}$, 2×1, 3×1 reconstructions and K vacancies. The crystal axes in panels (d)–(g) are consistent. (h)–(k) The $\mathrm{d}I/\mathrm{d}V$ spectra correspond to the structures depicted in panels (d)–(g), respectively. To ensure the representativeness of the spectra for the nanoscale 3×1 stripe and K vacancies, the spectra were acquired as much as possible within the well-defined, intact regions of these two structures, as indicated by the white dots in panels (f) and (g). (l) The gap values on different structures.

In addition to the superconducting gap, the spectra in Fig. 3(a) reveal two distinct density of states (DOS) peaks around -130 mV and -43 mV on the $\sqrt{2}\times\sqrt{2}$ surface, which we designate as peak 1 and peak 2, respectively. Figure 3(b) shows the evolution of these DOS peaks across different surface configurations. The 2×1 and $\sqrt{2}\times\sqrt{2}$ surfaces share the similar spectra, consistent with their equivalent carrier concentration and the comparable gap amplitudes, as discussed in Fig. 2. However, on the 3×1 and vacancy regions with lower K coverage, both DOS peaks show hole-doping behavior.

Figure 3(c) illustrates the correlation between peak 2 and the superconducting gap. It is evident that such flat-band-like DOS play a key role in modulating the gap values. As peak 2 gradually crosses the E_{F}, smaller gaps are induced in the 3×1 and K vacancy regions. This behavior closely resembles the VHS observed near the E_{F} (-4 meV) in the heavily hole-doped KFe_2As_2 (0.5 hole/Fe), where a corresponding suppression of superconductivity is seen compared to the optimally doped case (0.2 hole/Fe in $Ba_{0.6}K_{0.4}Fe_2As_2$).[35] Moreover, doping-depended electron correlation and a potential Mott state deep within the hole regime have been proposed in FeSCs phase diagram.[39–41] On the K12442 surface, the spectra background undergoes changes in parallel with the shift of DOS peaks, with particularly noticeable alterations observed above $+150$ meV, as highlighted by the line segments in Fig. 3(a). This indicates that the simple rigid band model is no longer applicable, and both the carrier filling and electron correlation must be considered simultaneously in the band structure.

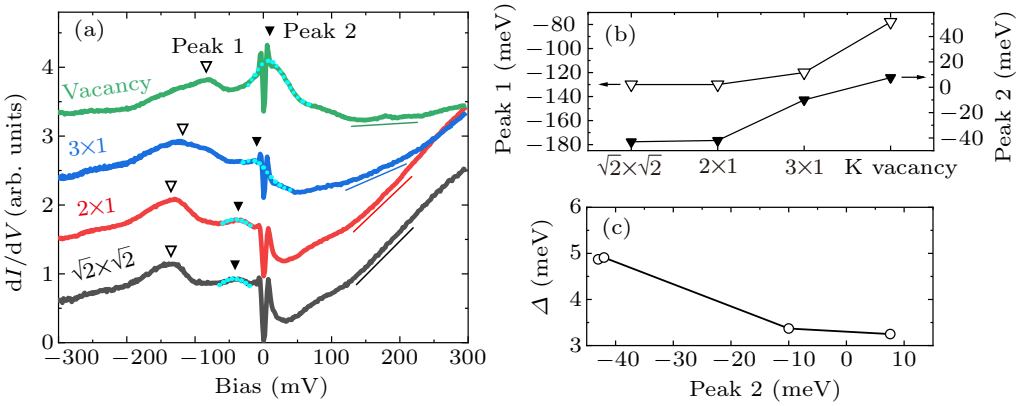


Fig. 3. (a) Typical spectra over a larger energy range measured on four different structures. The hollow and solid triangles represent the positions of two characteristic DOS peaks. The bright blue dotted line represents the Gaussian fitting of peak 2, highlighting its peak position. The line segment near +200 mV accentuates the variation in the spectra background. (b) A summary of the peak positions for peak 1 and peak 2 across four different regions. (c) The relationship between the superconducting gap and the position of peak 2.

By varying the K coverage, the isolated FeAs layer on K12442 surface evolves from its pristine state (0.25 hole/Fe) to higher hole doping, accompanied by changes in the overall electronic correlation. At the same time, the common characteristic of VHS in FeAs-based FeSCs is revealed. Current studies on the surfaces of FeSCs still need to consider the superconducting proximity effect, disorder, and the potentially complex interplay between surface reconstruction and magnetism.[20,26,42] The clear experimental results and qualitative discussions presented here are expected to offer boundary conditions and insights into these issues. In addition, guidelines for other surface-sensitive measurements are provided, emphasizing the need to fully consider the electronic structure and superconducting multiplicity in the mesoscopic regions targeted by photoemission spectroscopy and particle tunneling processes.

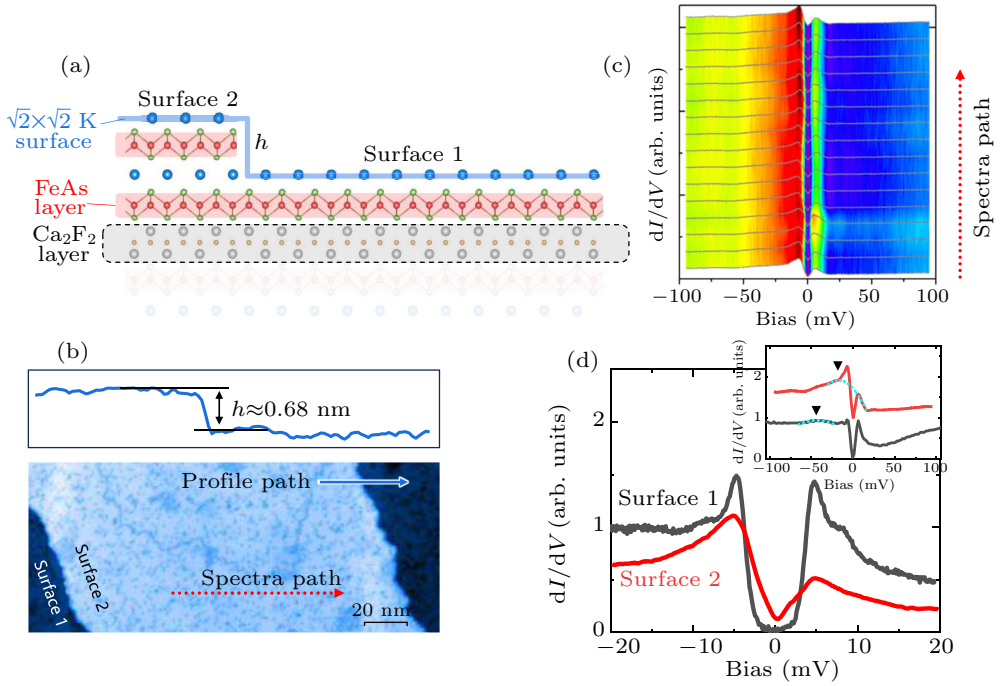


Fig. 4. (a) A cross-sectional schematic diagram of the K12442 cleavage surface. Surface 1 is the typical scenario, on which an FeAs monolayer is isolated from the bulk counterpart by the underlying CaF block; conversely, surface 2 is exceedingly rare, with a probability of being encountered during random scanning of less than 1‰. (b) The terrace of surface 2, featuring step edges. The step height ∼ 0.68 nm closes to the standard value of the structural model depicted in panel (a). (c) A series of spectra acquired at equidistant intervals along the dotted line on surface 2 in panels (b), which illustrates the uniformity of the spectra on surface 2. (d) Spectra on surfaces 1 and 2. The main panel displays spectra acquired with a small modulation voltage on both surface 1 and surface 2, facilitating detailed comparison of the superconducting gaps. The inset displays spectra acquired with a larger bias range on both surfaces 1 and 2. The black triangles in the inset denote the positions of the DOS peak 2, and the blue dotted lines represent the Gaussian fitting.

Finally, we investigate the bilayer structure on the K12442 surface. In Fig. 4, the surface 1 represents a common cleave surface, where the FeAs bilayer is separated, and the remaining FeAs monolayer is isolated from the bulk by the underlying CaF block, consistent with literature reports.[20] In fact, all the studies presented in Figs. 1–3 are conducted on this common surface 1. Interestingly, we occasionally observe a new surface, referred to as surface 2 in Fig. 4(a).

Through atomic-resolution topography and step-height analysis (Fig. 4(b)), it was identified as an FeAs bilayer covered with the $\sqrt{2}\times\sqrt{2}$ K lattice.

With the $\sqrt{2}\times\sqrt{2}$ K termination acting as a half-K layer, the FeAs monolayer on surface 1 maintains a similar doping level as the bulk counterpart (~ 0.25 hole/Fe). However, for surface 2, this half-K layer is distributed over the FeAs bilayer, resulting in a level of ~ 0.375 hole/Fe in the FeAs bilayer under simplified stoichiometry. This indicates a moderate hole doping on surface 2 relative to the pristine state. Figure 4(d) displays the typical spectra on these two types of surfaces. A DOS peak appears near E_F on surface 2, confirming the hole-doping behavior, which is similar to the scenario shown in Fig. 3 (the inset of Fig. 4(d)). More importantly, the superconducting gap on surface 2 exhibits a V-shaped structure, with elevated zero bias conductance. This suppression of superconductivity is distinctly different from that in Fig. 3. Considering the unique FeAs bilayer structure of surface 2, the gap splitting induced by the interlayer coupling may be responsible for the formation of this V-shaped gap.[28]

In summary, we have investigated the electronic state modulation on the quasi-2D K12442 surface. Striped structures and nanoscale K vacancies are revealed on the cryogenically cleaved surfaces. The reduction in K coverage qualitatively induces hole-doping behavior, but this phenomenon cannot be explained by a simple rigid-band scenario. The superconductivity is closely related to the VHS near the E_F, and its evolution can be understood as a result of the interplay between surface carriers and electronic correlations. Moreover, a V-shaped gap is observed on the surface that preserves the FeAs bilayer structure, which may be attributed to the FeAs interlayer coupling. The diversity of surface structures and electronic states on K12442 not only offers guidelines for other surface-sensitive measurements but also facilitates the modulation and application of the basic FeAs superconducting layer.

Acknowledgements

Project supported by the National Key Research and Development Program of China (Grant Nos. 2024YFA1611103 and 2022YFA1403203), the Innovation Program for Quantum Science and Technology (Grant Nos. 2024ZD0301300 and 2021ZD0302802), and the National Natural Science Foundation of China (Grant Nos. 12474128, 12374133, 12204008, and 12104004). We would like to thank H. Q. Luo for his fruitful discussions.

References

[1] Paglione J and Greene R L 2010 *Nat. Phys.* **6** 645
[2] Fernandes R M, Coldea A I, Ding H, Fisher I R, Hirschfeld P J and Kotliar G 2022 *Nature* **601** 35
[3] Yi M, Zhang Y, Shen Z X and Lu D H 2017 *Npj Quantum Mater.* **2** 57
[4] Kordyuk A A 2012 *Low Temp. Phys.* **38** 888
[5] Ishida S, Song D, Ogino H, Iyo A and Eisaki H 2017 *Phys. Rev. B* **95** 014517
[6] Canfield P C and Bud'ko S L 2010 *Ann. Rev. Condens. Matter Phys.* **1** 27
[7] Yamazaki T, Takeshita N, Kobayashi R, Fukazawa H, Kohori Y, Kihou K, Lee C H, Kito H, Iyo A and Eisaki H 2010 *Phys. Rev. B* **81** 224514
[8] Alireza P L, Ko Y T C, Gillett J, Petrone C M, Cole J M, Lonzarich G G and Sebastian S E 2009 *J. Phys.: Condens. Matter* **21** 012208
[9] Wen C H P, Xu H C, Chen C, Huang Z C, Lou X, Pu Y J, Song Q, Xie B P, Abdel Hafiez M, Chareev D A, Vasiliev A N, Peng R and Feng D L 2016 *Nat. Commun.* **7** 6433
[10] Niu X H, Chen S D, Jiang J, Ye Z R, Yu T L, Xu D F, Xu M, Feng Y, Yan Y J, Xie B P, Zhao J, Gu D C, Sun L L, Mao Q, Wang H, Fang M, Zhang C J, Hu J P, Sun Z and Feng D L 2016 *Phys. Rev. B* **93** 054516
[11] Wang Q Y, Li Z, Zhang W H, Zhang Z C, Zhang J S, Li W, Ding H, Ou Y B, Deng P, Chang K, Wen J, Song C L, He K, Jia J F, Ji S H, Wang Y Y, Wang L L, Chen X, Ma X C and Xue Q K 2012 *Chin. Phys. Lett.* **29** 037402
[12] Song C L, Zhang H M, Zhong Y, Hu X P, Ji S H, Wang L L, He K, Ma X C and Xue Q K 2016 *Phys. Rev. Lett.* **116** 157001
[13] Zhang C, Hu T, Wang T, Wu Y, Yu A, Chu J, Zhang H, Zhang X, Xiao H, Peng W, Di Z, Qiao S and Mu G 2021 *2D Mater.* **8** 025024
[14] Chang K, Deng P, Zhang T, Lin H C, Zhao K, Ji S H, Wang L L, He K, Ma X C, Chen X and Xue Q K 2015 *Europhys. Lett.* **109** 28003
[15] Ueda S, Yamagishi T, Takeda S, Agatsuma S, Takano S, Mitsuda A and Naito M 2011 *Physica C* **471** 1167
[16] Li M, Li G, Cao L, Zhou X T, Wang X C, Jin C Q, Chiu C K, Pennycook S J, Wang Z Q and Gao H J 2022 *Nature* **606** 890
[17] Nag P K, Scott K, De Carvalho V S, Byland J K, Yang X Z, Walker M, Greenberg A G, Klavins P, Miranda E, Gozar A, Taufour V, Fernandes R M and Da Silva Neto E H 2024 *Nat. Phys.* **21** 89
[18] Gao M, Ma F J, Lu Z Y and Xiang T 2010 *Phys. Rev. B* **81** 193409
[19] Liu W Y, Cao L, Zhu S Y, Kong L Y, Wang G W, Papaj M, Zhang P, Liu Y B, Chen H, Li G, Yang F Z, Kondo T, Du S X, Cao G H, Shin S, Fu L, Yin Z P, Gao H J and Ding H 2020 *Nat. Commun.* **11** 5866
[20] Shao S, Zhang F, Zhang Z Y, Wang T, Wu Y W, Tu Y B, Hou J, Hou X Y, Hao N, Mu G and Shan L 2023 *Sci. China-Phys. Mech. Astron.* **66** 287412
[21] Duan W, Chen K L, Hong W S, Chen X Y, Yang H, Li S L, Luo H Q and Wen H H 2021 *Phys. Rev. B* **103** 214518
[22] Stolyarov V S, Pervakov K S, Astrakhantseva A S, Golovchanskiy I A, Vyalikh D V, Kim T K, Eremeev S V, Vlasenko V A, Pudalov V M, Golubov A A, Chulkov E V and Roditchev D 2020 *J. Phys. Chem. Lett.* **11** 9393
[23] Koepernik K, Johnston S, Heumen V, Huang Y, Kaas J, Goedkoop J B, Golden M S and Brink J V D 2012 *Phys. Rev. Lett.* **109** 127001
[24] Li A, Yin J X, Wang J H, Wu Z, Ma J H, Sefat A S, Sales B C, Mandrus D G, McGuire M A, Jin R Y, Zhang C L, Dai P C, Lv B, Chu C W, Liang X J, Hor P H, Ting C S and Pan S H 2019 *Phys. Rev. B* **99** 134520
[25] Yin J X, Wu X X, Li J, Wu Z, Wang J H, Ting C S, Hor P H, Liang X J, Zhang C L, Dai P C, Wang X C, Jin C Q, Chen G F, Hu J P, Wang Z Q, Li A, Ding H and Pan S H 2020 *Phys. Rev. B* **102** 054515
[26] Hu Q X, Yang F Z, Wang X Y, Li J J, Liu W Y, Kong L Y, Li S L, Yan L, Xu J P and Ding H 2023 *Phys. Rev. Mater.* **7** 034801
[27] Zhang H, Dai J, Zhang Y J, Qu D R, Ji H W, Wu G, Wang X F, Chen X H, Wang B, Zeng C G, Yang J L and Hou J G 2010 *Phys. Rev. B* **81** 104520
[28] Wu D S, Hong W S, Dong C X, *et al.* 2020 *Phys. Rev. B* **101** 224508
[29] Pyon S, Kobayashi Y, Takahashi A, Li W J, Wang T, Mu G, Ichinose A, Kambara T, Yoshida A and Tamegai T 2020 *Phys. Rev. Mater.* **4** 104801
[30] Wang Z C, He C, Wu S Q, Tang Z T, Liu Y, Ablimit A, Feng C M and Cao G H 2016 *J. Am. Chem. Soc.* **138** 7856
[31] Chen X Y, Duan W, Fan X W, Hong W S, Chen K L, Yang H, Li S L, Luo H Q and Wen H H 2021 *Phys. Rev. Lett.* **126** 257002
[32] Hou Z Y, Chen K L, Hong W S, Wang D, Duan W, Yang H, Li S L, Luo H Q, Wang Q H, Xiang T and Wen H H 2025 *Phys. Rev. X* **15** 011027

[33] Hong W S, Song L X, Liu B, Li Z Z, Zeng Z Y, Li Y, Wu D S, Sui Q T, Xie T, Danilkin S, Ghosh H, Ghosh A, Hu J P, Zhao L, Zhou X J, Qiu X G, Li S L and Luo H Q 2020 *Phys. Rev. Lett.* **125** 117002

[34] Wang Z C, Liu Y, Wu S Q, Shao Y T, Ren Z and Cao G H 2019 *Phys. Rev. B* **99** 144501

[35] Fang D L, Shi X, Du Z Y, Richard P, Yang H, Wu X X, Zhang P, Qian T, Ding X X, Wang Z Y, Kim T K, Hoesch M, Wang A F, Chen X H, Hu J P, Ding H and Wen H H 2015 *Phys. Rev. B* **92** 144513

[36] Wang T, Chu J N, Jin H, Feng J X, Wang L L, Song Y K, Zhang C, Xu X G, Li W, Li Z J, Hu T, Jiang D, Peng W, Liu X S and Mu G 2019 *J. Phys. Chem. C* **123** 13925

[37] Duan W, Chen K L, Hong W S, Chen X Y, Li S L, Luo H Q, Yang H and Wen H H 2022 *Nano Lett.* **22** 9450

[38] Li P, Liao S, Wang Z C, Li H X, Su S W, Zhang J K, Chen Z Y, Jiang Z C, Liu Z T, Yang L X, Huai L W, He J F, Cui S T, Sun Z, Yan Y J, Cao G H, Shen D W, Jiang J and Feng D L 2024 *Nat. Commun.* **15** 6433

[39] Liu X, Tao R, Ren M Q, Chen W, Yao Q, Wolf T, Yan Y J, Zhang T and Feng D L 2019 *Nat. Commun.* **10** 1039

[40] De'Medici L, Giovannetti G and Capone M 2014 *Phys. Rev. Lett.* **112** 177001

[41] Li J, Zhao D, Wu Y P, Li S J, Song D W, Zheng L X , Wang N Z, Luo X G, Sun Z, Wu T and Chen X H 2016 arxiv.org/abs/1611.04694

[42] Li G, Liang L, Li Q, Pan M, Nascimento V B, He X, Karki A B, Meunier V, Jin R, Zhang J and Plummer E W 2014 *Phys. Rev. Lett* **112** 077205